The Relationship between Centaur Activity and Ring Formation

by

Sophia E. Tigges

Submitted to the Department of Earth, Atmospheric and Planetary Sciences
in Partial Fulfillment of the Requirements for the Degree of

Bachelor of Science
at the
Massachusetts Institute of Technology

February 2018

Signature of Author ..... Signature redacted .....
Department of Earth, Atmospheric and Planetary Sciences
January 8, 2018

Certified by ..... Signature redacted .....
Amanda S. Bosh
Senior Lecturer in Earth, Atmospheric and Planetary Sciences
Thesis Supervisor

Certified by ..... Signature redacted .....
Margaret Pan
Research Scientist in Earth, Atmospheric and Planetary Sciences
Thesis Supervisor

Accepted by ..... Signature redacted .....
Richard P. Binzel
Professor of Earth, Atmospheric and Planetary Sciences
Chair, Undergraduate Committee

Introduction

Centaurs are small bodies whose orbits lie between those of Jupiter and Neptune (Gehrels, 1999). They are thought to be transition objects that originate in the Kuiper belt and occupy the cis-Neptunian region before potentially becoming Jupiter-family or other short-period comets (Dones, Levison, & Duncan, 1996). Their short dynamical lifetimes are on the order of 10^6 years (Horner, Evans, & Bailey, 2004) due to their unstable, planet-crossing orbits (Horner, Evans, Bailey, & Asher, 2003). Some Centaurs have been observed to be active, and the bodies in the population of active Centaurs have perihelion distances that are statistically smaller than the median perihelion distance for all Centaurs, suggesting that Centaur activity is thermal in nature (Jewitt, 2009).

Centaur activity may be observed through changes in the brightness of an object such as those exhibited by the Centaur Chiron (Parker et al., 1997). The presence of a coma around a Centaur may also provide evidence of activity, and dust comae have been detected around several bodies including Chiron (Meech & Belton, 1989; Luu & Jewitt, 1990) and Echeclus (Choi, Weissman, & Polishook, 2006). In addition to comae, other structures have been observed around Centaurs, such as the ring system that was discovered around Chariklo during a stellar occultation (Braga-Ribas et al., 2014). A symmetric feature was observed around Chiron during an occultation (Ruprecht et al., 2015), and some interpret this feature to be possible ring material (Ortiz et al., 2015). Similarly, the trans-Neptunian dwarf planet Haumea was revealed to have a ring during a stellar occultation (Ortiz et al., 2017).

The collisional spreading time of Chariklo's rings was calculated to be on the order of 10^5 years, which is short in comparison to the estimated Centaur lifetime of approximately 10^6 years (Pan & Wu, 2016), yet Centaur rings are still observed despite this contradiction. Shepherd satellites may serve to increase the lifetime of a Centaur's rings (Pan & Wu, 2016) and maintain distinct ring edges such as those observed in Chariklo's ring system (Charnoz, Canup, Crida, & Dones, 2017). Moreover, Centaur activity could supply material to an already present ring system, thus prolonging its lifetime. This study explores the potential connection between Centaur activity and Centaur ring systems by using the N-body integrator REBOUND to model outburst particle interactions and distributions.

Background

Centaurs are likely composed of a combination of volatile ices and silicate materials (Luu & Jewitt, 1996). Activity perhaps results from the sublimation of these volatile components (Parker, Stern, Festou, A'Hearn, & Weintraub, 1997), and these processes could produce local gas jets and dispersed outgassing events (Brown & Luu, 1998). These outbursts may cause dust particles to leave the body's surface (Parker et al., 1997), and these particles may fall back to the surface, remain in orbit, or escape. Factors that may influence the fate of these particles include the mass and radius of the Centaur, the mass and radius of the particles, the nature of the outburst, and the presence of a satellite or of previously lofted material around the Centaur.

Several mechanisms have been proposed for ring formation around these small bodies, including the excavation of material by collisions, the tidal disruption of a satellite, and the lofting of material due to activity (Pan & Wu, 2016). Furthermore, debris could be created through mantle stripping during a close encounter with a giant planet (Hyodo, Charnoz, Genda, & Ohtsuki, 2016) or during a three-body encounter between the small body and two field objects (Melita, Duffard, Ortiz, & Campo-Bagatin, 2017).

Though activity and particle structures have been observed for Centaurs, the formation and the time evolution of these structures have not been extensively explored. Dust particles may be lofted off the surface of a Centaur during activity (Pan & Wu, 2016), and these particles may fall back to the surface, remain in orbit around the body, or escape. The dust particles are disturbed by gas that is produced by volatile sublimation and is traveling at the sound speed (Finson & Probstein, 1968). This gas sound speed is dependent on the temperature and density of the medium, rendering the body's distance from the sun relevant to the velocity of the dust particles. The particles are also subject to gravitational and drag forces, which are dependent on the mass and radius of the Centaur, the density and radius of the particles, and the density of the medium. The velocity of the outburst particles due to the body's rotation adds a component to the total velocity of the outburst particles. The magnitude of this component depends on the rotation period of the body and the distance of the outburst from the body's axis of rotation.

Considering the balance of the forces that a dust particle experiences, a particle that leaves the surface of the body at a velocity less than the escape velocity will fall back to the body's surface. If the velocity of the particle is greater than or equal to the escape velocity, the particle will escape. However, collisions between particles can cause these particles to remain in orbit around the body (Pan & Wu, 2016). The likelihood of collisions depends on the optical depth of the outflow and of the material that may already be present around the body. Optical depth is determined by particle cross sectional area and number density. The gravitational influence of the dust particles on one another is also a consideration when examining particle interactions, and these forces depend on particle mass and radius.

Several other factors are important to the form of the outburst and the subsequent distribution of dust particles. The location and expanse of the activity, such as localized activity from a patch or more diffuse activity from a larger region, influence the morphology of the outburst. The outburst's velocity and expanse contribute to its strength, which serves an important role if the outflow must travel past or through overlying material. The direction of the outburst governs the incidence angle of the particles on any material that may surround the body. Finally, the outburst duration, which could be continuous or sporadic, governs the contribution of the outburst particles to the material already surrounding the body and affects the likelihood of particle interactions.

Because Centaur activity is suspected to be thermal in nature (Jewitt, 2009), composition is also relevant to the discussion of this outburst activity. Although the composition of the bodies is largely unknown, they are expected to posses a silicate interior surrounded by a volatile-rich mantle (Hyodo et al., 2016). A non-volatile crust may be present on the body's exterior due to irradiation. Such a crust may be present on Kuiper belt objects and consequently on Centaurs, and this crust may prevent the sublimation of volatile materials beneath it (Luu & Jewitt, 1996).

Centaurs are suggested to have compositions similar to those of observed Kuiper belt objects or short-period comets. Kuiper belt objects likely contain molecular ices, including H_2O, CO, CO_2, and N_2 ices (Luu & Jewitt, 1996), while short-period comets consist of similar ices as well as CH_4, HCN, CH_3OH, and NH_3 ices (Romanishin, Tegler, Levine, & Butler, 1997). Spectral observations of Centaurs confirm some of these expectations. Water ice has been detected in the spectra of bodies such as Bienor (Barkume, Brown, & Schaller, 2008), Chiron (Foster, Green, McBride, & Davies, 1999), and perhaps Chariklo, in which case it may be associated with the body's rings (Duffard et al., 2014). The presence of CN (Bus, A'Hearn, Schleicher, & Bowell, 1991) and of CO (Womack & Stern, 1997) has also been noted in Chiron's coma, suggesting that these volatiles are involved in the body's activity. However, a

body's active volatiles may vary over the course of an orbit based on distance from the sun and over longer timescales due to the depletion of volatile reservoirs or the evolution of the body's orbit.

Additionally, the arrangement of silicate and volatile materials within the structure of the Centaur may affect the sublimation of the volatile ices. Previous activity may expose volatiles below the surface, allowing for further sublimation. Furthermore, the porosity of overlying material determines the ability of the underlying volatiles to escape, influencing the form of the resulting outflow. Previous bouts of activity could cause weakening or produce void space within the body's structure, allowing more material to escape during subsequent episodes of activity and perhaps changing the form of the outflow during these later episodes.

Because little is known about the structure and composition of the active Centaurs, modeling these elements poses a challenge. However, simulating the kinematic aspects of activity is more straightforward, and REBOUND is better suited to such modeling. Thus, this study focuses on the kinematics of Centaur activity and its implications for ring formation or replenishment.

Methods

The Python package of the N-body integrator REBOUND was used to study the behavior of particles launched from the surface of a body with the characteristics of Chiron. REBOUND's design focuses on collisional dynamics, and its applications include the study of planetary ring systems. The hermes integrator was used with the direct collision detection module and with a free-slip, hard-sphere collision model (Rein & Liu, 2012). The choices made for the setup of the simulations performed in REBOUND are summarized below in Table 1.

Table 1
REBOUND Setup

REBOUND Characteristic	Choice Used for Simulations	
Version	3.5.4	
Integrator	hermes	
Collision module	direct	
Collision resolving routine	hardsphere	
Box size	148×10^6 m	
Coordinate system	Ring	Keplerian
	Outflow	Cartesian
Units	SI	

Additionally, a setup scheme was required in order to represent the geometry of the outflow with relation to the body. A top-down view of this setup, the geometry of which is entirely contained within the xy-plane, is shown in Figure 1. In all trials, the outburst occurred at the equator of the body, and all launch geometry occurs in the equatorial plane. The outburst location along the equator was specified by the central angle α measured from the horizontal. For trials in which the outburst occurred from a patch rather than from a point, the active area was bounded by a chosen angle range in order to encompass the desired patch area. In such cases, the initial position of each particle was chosen randomly from the specified swath. The velocity of each test particle was chosen randomly from a given range of velocities for each trial. The angle

of the outburst relative to the surface of the body was described by a second angle β measured from the vertical at the outburst location.

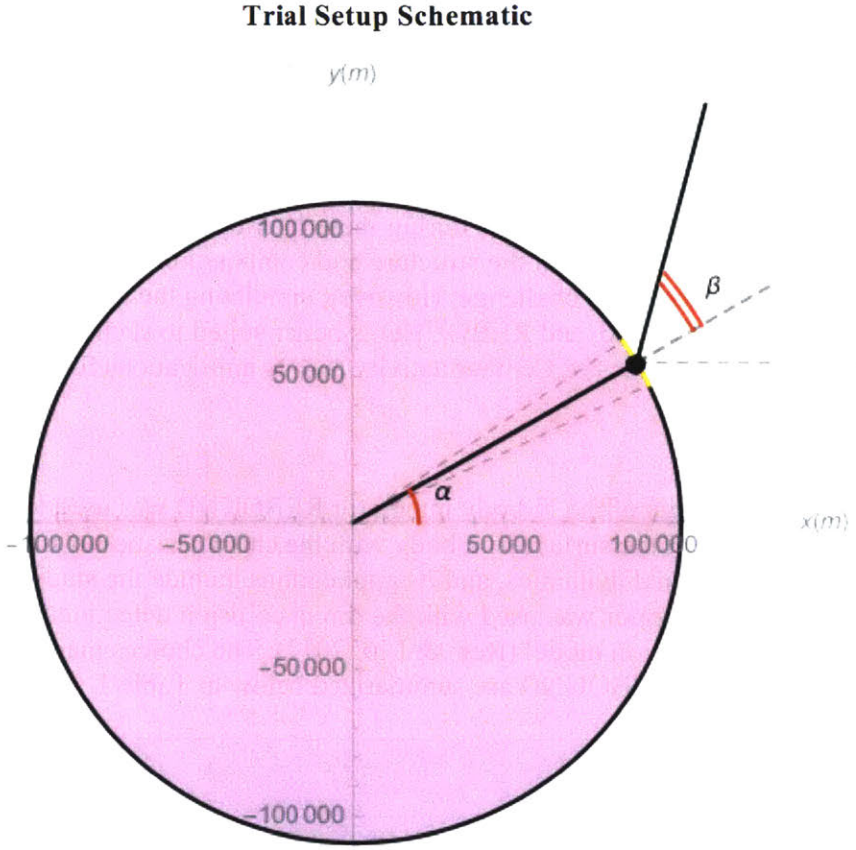

Figure 1. Schematic diagram depicting setup for trials run in REBOUND. The setup is shown in plan view with the x- and y-axes labeled in meters. In this top-down view, the body is depicted in lavender. The outburst was located at the equator for all trials. The location of the outburst was described by the angle α measured from the horizontal. In patch cases, the x- and y-positions of the outburst particles were chosen from a range to either side of the equatorial point specified by α, and this area is shown in yellow along the body's surface. The angle of the outburst was specified by the angle β measured from the vertical at the outburst location specified by α.

Chiron was chosen as a representative body for the Centaur population, and Chiron's characteristics were used in the calculations and simulations completed for this study. Chiron has been observed to be active, exhibiting observable increases in brightness (Parker et al., 1997) in conjunction with this activity. Additionally, the dust coma (Jewitt, 2009) and the other material present around the body (Ruprecht et al., 2015 and Ortiz et al., 2015) suggest that there may be a relationship between the body's activity and the particle structures that surround it. The universal values used in the REBOUND simulations, including the values that follow from the choice of

Chiron as a representative body, are summarized below in Table 2. The calculations used to obtain the values for the gas sound speed and the escape velocity can be found in Appendix A.

Table 2
Universal Values Used for REBOUND Simulations

Characteristic	Value	
Centaur parameters	Mass[1]	10^{19} kg
	Radius[2]	109 x 10^3 m
	Perihelion distance[3]	8.43 AU
	Rotation period P[3]	5.918 h
Escape velocity[4]	110.7 m/s	
Sound speed[4]	1123.4 m/s	
Effects of sunlight	none	

[1]Williams, 2014.
[2] Fornasier et al., 2013.
[3]Jet Propulsion Laboratory Small-Body Database Browser, n.d.
[4]The calculations made to obtain these values can be found in Appendix A.

As previously mentioned, the velocity of an outflow particle determines whether the particle escapes or returns to the body's surface. To demonstrate the effects of initial particle velocity on the orbits of the outflow particles, some example plots were generated in REBOUND to depict particle orbits for different launch velocities (Figure 2). These plots depict the instantaneous orbits of outburst particles in the xy-plane. The particles are all launched from an equatorial point on the body's surface. Note that a particle's instantaneous orbit is distinct from the particle's trajectory. Additionally, bear in mind that the body's mass is taken to be concentrated at a point at the body's center, which is represented by the star in the figure.

The red example orbit shows a particle with a launch velocity an order of magnitude less than the escape velocity, and this particle returns to the body's surface almost immediately after launch, as seen in the inset in Figure 2. The blue example orbit shows a particle with a launch velocity on the order of the escape velocity, and it has a highly eccentric orbit but still returns to the surface of the body. The orange example orbit shows the instantaneous orbit of a particle with a launch velocity between that of the red orbit and that of the blue orbit. This particle falls back to the surface of the body, but not as immediately as the particle represented by the red orbit, and with an instantaneous orbit not quite as eccentric as that of the particle represented by the blue orbit. The magenta orbit depicts the path of a particle for which magnitudes of the launch velocity and the rotational velocity sum to the escape velocity. As a result, the orbit of this particle is a parabola with an eccentricity equal to 1. The chartreuse orbit shows the instantaneous orbit of a particle launched at a velocity on the order of one half of the gas sound speed. This orbit is hyperbolic and thus unbound. In addition to illustrating the significance of the initial velocity in terms of the instantaneous orbits of the outburst particles, these example plots also show the importance of interactions between particles that alter particle trajectories and cause material to remain in orbit around the body.

Sample Instantaneous Orbits for Outflow Particles with Varying Initial Velocities

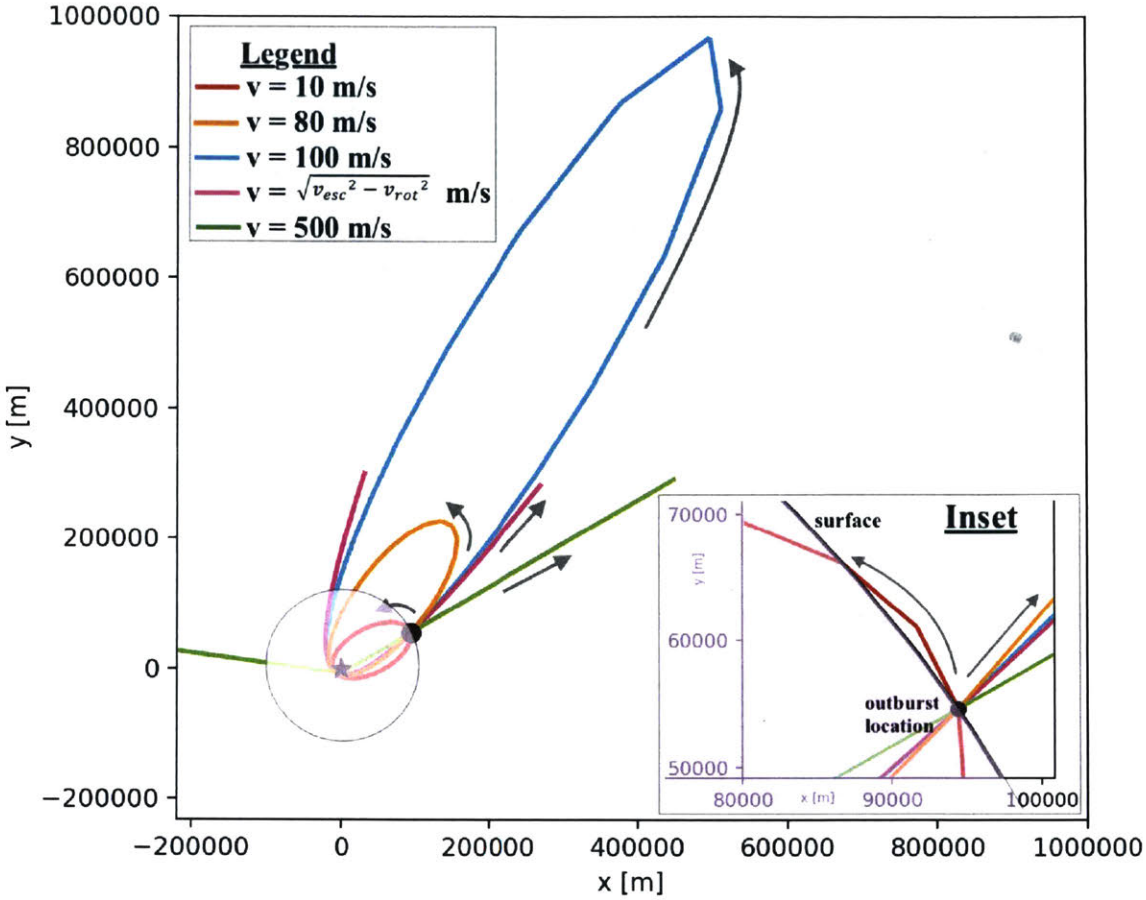

Figure 2. Plan view of sample instantaneous orbits for outflow particles with varying initial velocities. Note that a particle's instantaneous orbit it distinct from its trajectory. The Centaur body is shown in lavender. The Centaur's mass is concentrated at its center, which is represented by the star. The particles are launched from an equatorial point at the surface represented by the dot. The arrows show the direction of motion of the particles. The inset shows a more detailed view of the outflow point and the body's surface in its vicinity. The instantaneous orbits that are shown correspond to outflow particles with the following initial velocities: red, v_i = 10 m/s; orange, v_i = 80 m/s; blue, v_i = 100 m/s (slightly less than the escape velocity); magenta, $v_i = \sqrt{v_{esc}^2 - v_{rot}^2} = 105.9$ m/s (launch and rotational components of velocity add exactly to v_{esc}); chartreuse, v_i = 500 m/s $\sim \frac{1}{2} v_{esc}$.

The remaining methods as well as the results will be broken into two sections based on the two sets of trials conducted for this study.

I. Outflow Particle Collision Trials

A brief first set of trials was conducted in REBOUND to assess the ability of collisions between outburst particles to produce particles that remained in orbit around the body (Appendix B). Thus, this set of trials was designed to make particle collisions favorable. In these trials,

particles were launched from the body's surface in a sporadic outburst with a fixed time interval. The optical depth of the outflow was of order unity. The values used for the setup of these trials are summarized in Table 3. The number of collisions that occurred between particles and the number of particles that remained in orbit around the body after the outburst were both counted.

Table 3
Values Used for Outflow Particle Collision Trials

Characteristic	Value	
Outflow particle parameters	Density	1000 kg/m^3
	Mass	4.19 x 10^3 kg
	Radius	1 m
Number of outflow particles	Per burst	100
	Total	1200
Optical depth of outflow $\tau_{outflow}$	0.3	
Velocity range of outflow	x-component	0 m/s to 200 m/s
	y-component	0 m/s to 200 m/s
Time between bursts	10 s	
Total integration time	100 s	

II. Ring Collision Trials

A more extensive second set of trials evaluated the ability of collisions between outburst particles and ring material already present around the body to produce particles that remained in orbit after the outburst (Appendix C). Whereas the objective of the first set of trials was to maximize the number of mutual collisions between outflow particles to determine whether such collisions could produce particles that remained in orbit around the body, the aim of the second set of trials was to maximize the number of particles that remained in orbit around the body through collisions with present ring material. In this second set of trials, the initial velocities of the particles and the incidence angle of the outflow on the ring material were varied in order to search for a relationship between these parameters and the number of outflow particles that remained in orbit around the body at the end of each trial.

The values chosen for each parameter are summarized below in Table 4. The ring used in the simulation was modeled after measurements made of Chariklo's ring (Braga-Ribas et al., 2014). The ring lies completely within the equatorial plane and has a thickness equal to the thickness of the particles of which it is comprised. Due to limitations in the total number of particles that could be used for each simulation, only a slice of ring material was used for each trial. In simulation, this ring slice was positioned so that the outflow particles would encounter it. Particles with a radius of one micron issuing from an active point at the equator were set up to collide with the particles in the ring slice after ejection. The number of collisions between outflow particles and ring particles, the number of particles that remained in orbit around the body after the outburst, the number of particles that fell back to the body's surface, and the number of particles that escaped were counted for each combination of initial velocity and incidence angle.

Table 4
Values Used for Ring Collision Trials

Characteristic	Value	
Outflow particle parameters	Density	1000 kg/m^3
	Mass	4.19 x 10^{-3} kg
	Radius[1]	10^{-6} m
Number of outflow particles	100	
Velocity range of outflow	0 m/s to 200 m/s	
Incidence angle range of outflow β	0° to 90°	
Ring particle parameters	Density	1000 kg/m^3
	Mass	4.19 x 10^9 kg
	Radius	100 m
Ring parameters	Orbital radius[2]	390 km
	Radial width[2]	6 km
Optical depth of ring τ_{ring}	0.3	
Total integration time	P	

[1]Note: The radius of the outflow particles was chosen with the intention of later adding the effects of radiation pressure to the simulation. Although radiation pressure was not accounted for in the simulations carried out for this study, micron-sized outflow particles were still used for this set of trials.

[2]Note: The ring created around Chiron was based on the innermost of Chariklo's two rings using the values measured by Braga-Ribas et al., 2014 instead of using the measurements of Chiron's possible rings made by Ortiz et al., 2015. This choice may be justified by the similar masses and diameters of the two bodies and by the better-studied nature of Chariklo's rings.

Prior to conducting this second set of trials, a simulation of the possible ring material surrounding Chiron was performed by representing this ring as a shearing sheet with an epicyclic frequency equal to that of a ring at an orbital radius of 390 km (Table 4). A patch of this shearing sheet was then integrated for one, two, five, and ten orbits of the ring around the body (Figure 3 and Appendix D). The parameters used for this simulation were the same as those listed in Table 1 except for the ring particle radii, which were chosen from the range of 1 meter to 4 meters with a power law distribution. Significant clumping appears to occur between the ring particles in the time between one and five orbits , but this clumping appears to remain approximately the same in the time between the five and ten orbits.

Some limitations in terms of the total number of particles that could be used in the simulation were faced in the ring collision trials. Given these limitations, the ring particles were required to be 100 meters in radius in order to achieve the desired optical depth due to the corresponding scaling relationship. The shearing sheet simulations show that particle clumps in the ring can grow to diameters of 50 meters within five to ten orbits. Although the ring particles used in the ring collision trials have diameters that are four times as large, the shearing sheet examples show that this chosen value does not seem to be unreasonable.

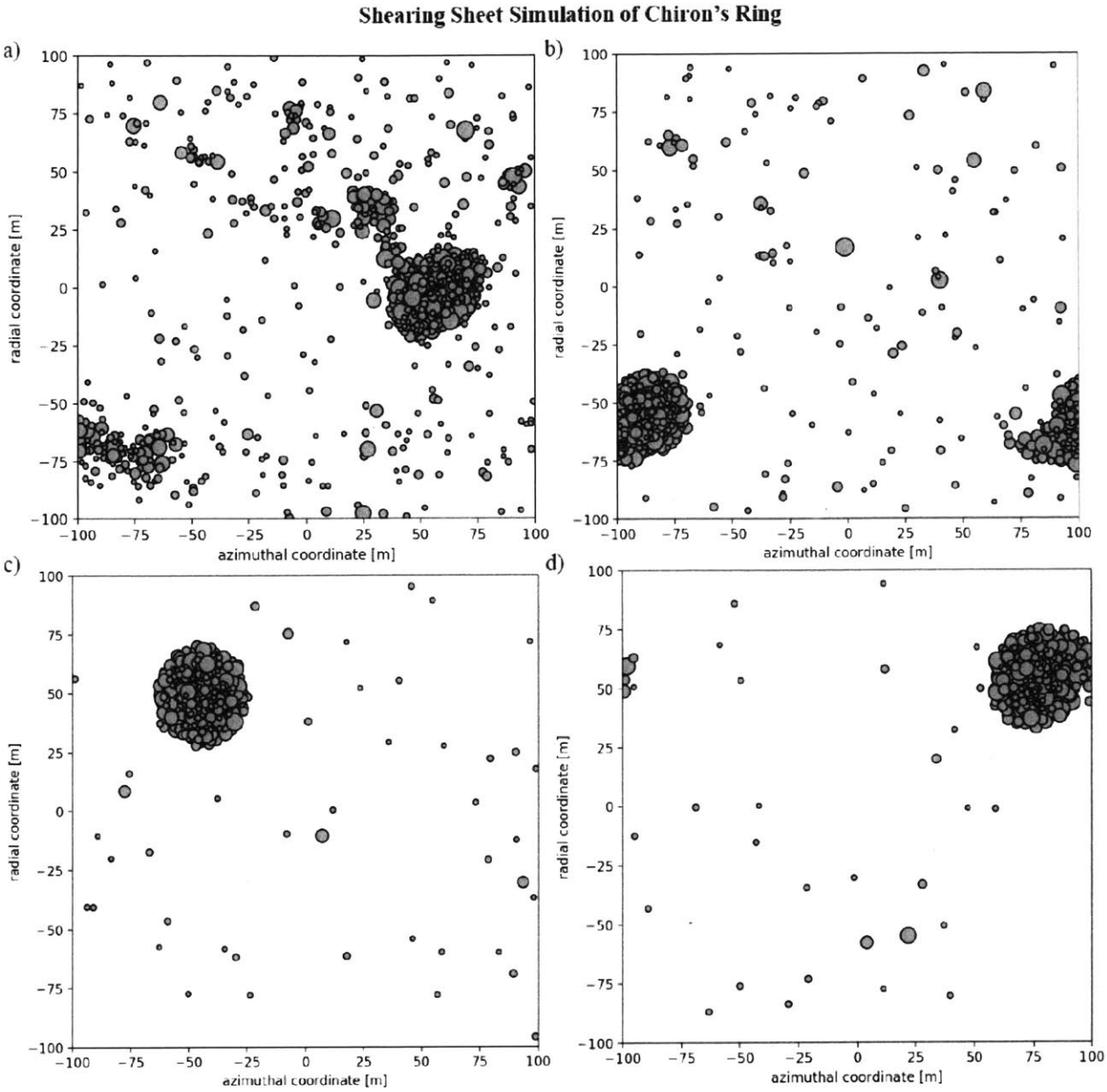

Figure 3. Shearing sheet simulation of Chiron's ring material. The simulation was integrated for one orbit (a), two orbits (b), five orbits (c), and ten orbits (d) of the ring around the body.

Results and Analysis

I. Outflow Particle Collision Trials

The first brief set of trials simulated a sporadic outburst with an optical depth of order unity issuing from a patch (Table 3) in order to make collisions between outflow particles favorable. Particle positions were selected randomly from a surficial patch located at the equator, and the x- and y-components of the initial particle velocities were each chosen randomly from the range of 0 m/s to 200 m/s. The number of particles that underwent collisions and the number

of particles that remained in orbit around the body were counted, and the results of these trials are contained in Table 5.

In the ten trials that were conducted, the mean number of particles that underwent collisions was 413.5 particles out of a total of 1200 particles included in the simulation, or 34.46% of particles. This value is close to the expected value of approximately 30% for the optical depth $\tau_{outflow}$=0.3 that was used. Out of all ten of the trials, one particle remained in orbit in two of the trials, which amounts to a mean of 0.02% of outflow particles remaining in orbit around the body due to interactions with other outflow particles. The rest of the particles in these trials either fell back to the body's surface or escaped.

However, these trials are limited in their scope. They do not test different optical depths, patch sizes, outburst morphologies, and outburst intervals, and variations of these characteristics could produce more collisions and consequently result in a greater number of outflow particles that orbit the body. Although these trials were not extensive in nature, they demonstrate the difficulty of producing material that remains in orbit around a small body through mutual particle collisions within an outflow. One fiftieth of one percent of particles remain in orbit around the body due to mutual collisions between outflow particles; while ring formation through such collisions cannot be entirely discounted, it is challenging to produce enough material around the body to form a ring through mutual collisions between outflow particles.

Table 5
Results of Outflow Particle Collision Trials

Trial Number	Particles that Underwent Collisions		Particles that Remained in Orbit	
	Number	Percentage	Number	Percentage
1	462	38.50%	0	0.00%
2	392	32.67%	0	0.00%
3	365	30.42%	0	0.00%
4	423	35.25%	0	0.00%
5	441	36.75%	1	0.08%
6	400	33.33%	0	0.00%
7	418	34.83%	0	0.00%
8	393	32.75%	0	0.00%
9	451	37.58%	0	0.00%
10	390	32.50%	1	0.08%
Mean	413.50	34.46%	0.20	0.02%
Median	409.00	34.08%	0.00	0.00%

II. Ring Collision Trials

The second set of trials aimed to produce material that remained in orbit around the body due to collisions with ring material that was already present (Table 4). The initial outflow velocity and the incidence angle of the outflow on the ring were varied between these trials. Phase space was partitioned by dividing initial outflow velocity into four ranges and by naming seven different incidence angle values.

The magnitude ranges for the initial velocity of each particle were 0 m/s to 50 m/s, 50 m/s to 100 m/s, 100 m/s to 150 m/s, and 150 m/s to 200 m/s. For each trial, the initial velocity of each particle was selected randomly from within the range used for the trial. The incidence angle

values used for the trials were 0°, 15°, 30°, 45°, 60°, 75°, and 90°. For each trial, the incidence angle was fixed at one of these values. For each combination of outflow initial velocity and incidence angle, the number of particles that collided with the ring, remained in orbit after a collision with the ring, fell back to the surface, and escaped were counted. The results of this second set of trials are summarized in Figures 4 through 8. Because each trial was run one time with 100 particles, the nominal error on all raw values given can be taken to be $\sqrt{N} = \pm 10$.

In these trials, increasing outflow velocities appear to produce more collisions between outflow particles and the ring material (Figure 4). Particle with velocities under 50 m/s do not reach the ring and therefore cannot collide with it. Outflow velocities greater than 100 m/s and incidence angles within the range of 30° to 60° resulted in the most collisions between outflow particles and the ring (Figure 4). However, velocities within the range of 50 m/s to 150 m/s produced the greatest number of outflow particles that remained in orbit after collision (Figure 5). A 45° incidence angle in combination with a velocity range of 50 m/s to 100 m/s caused 4 outflow particle to collide with the ring and subsequently remain in orbit. Although this trial resulted in the greatest number of outflow particles to remain in orbit after collision, the trial with an incidence angle of 90° and a velocity range of 50 m/s to 100 m/s produced one particle that collided with the ring and then remained in orbit. This trial represents the highest percentage of outflow particles that remain in orbit out of the total number that collided with the ring, but perhaps the significance of this finding is questionable due to the consideration of only one particle (Figure 6).

Because the edge-on optical depth of the ring was set to $\tau_{ring} = 0.3$, approximately 30% of the particles were expected to collide with the ring during each trial. Variations in the incidence angle as well as the uncertainty of ± 10 were expected to alter this percentage. For the simulations in which the outflow velocity is greater than 100 m/s and the particles reach the ring, the range of 11% to 34% of particles that collided with the ring falls within these expectations. The optical depth of the ring as seen from incidence angles of 0° to 60° must be close enough to the $\tau_{ring} = 0.3$ values to produce collisions for 19% to 34% of the particles. On the other hand, for the incidence angles of 75° to 90°, the effective optical depth of the ring must be closer to $\tau_{ring} = 0.10$ to 0.2 in order to produce the 11% to 20% of collisions that occurred.

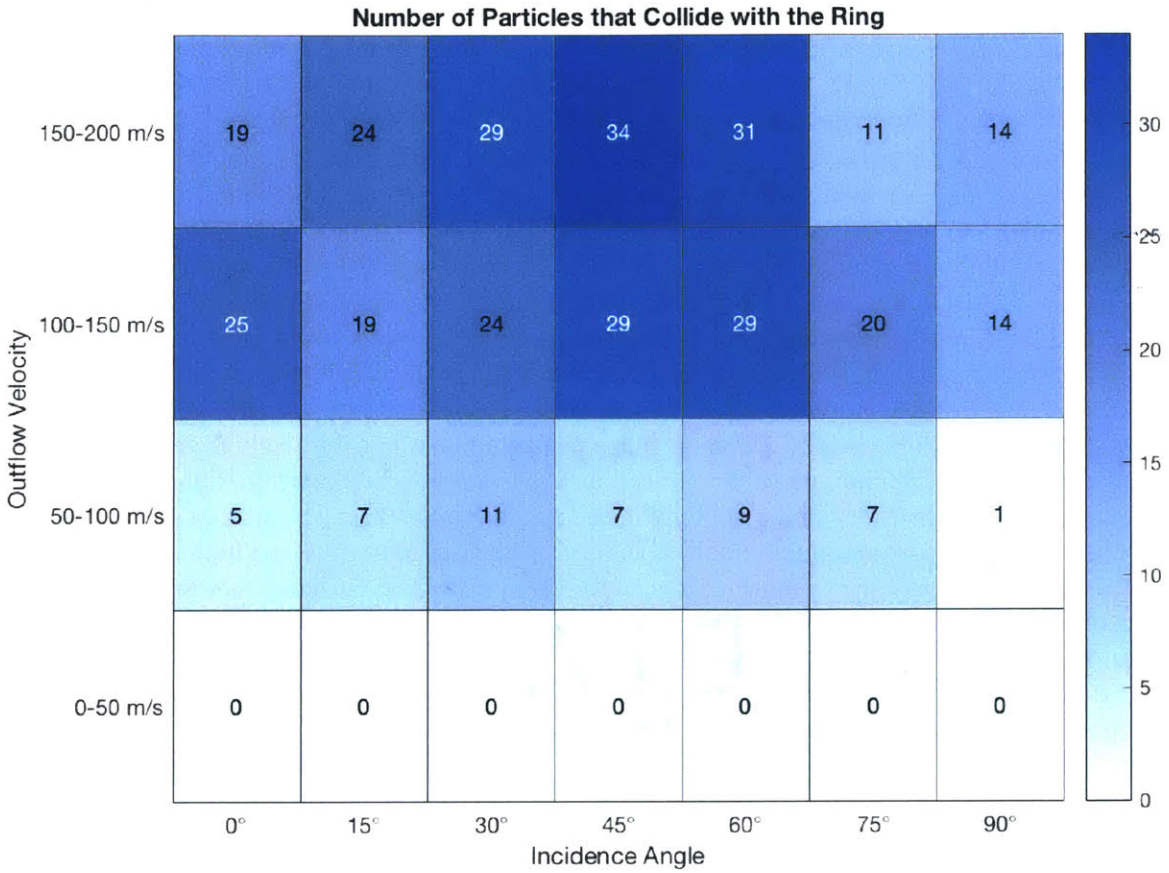

Figure 4. The number of outflow particles that collide with the ring material. For each trial conducted with 100 total outflow particles, the number of outflow particles that collided with the ring material is given.

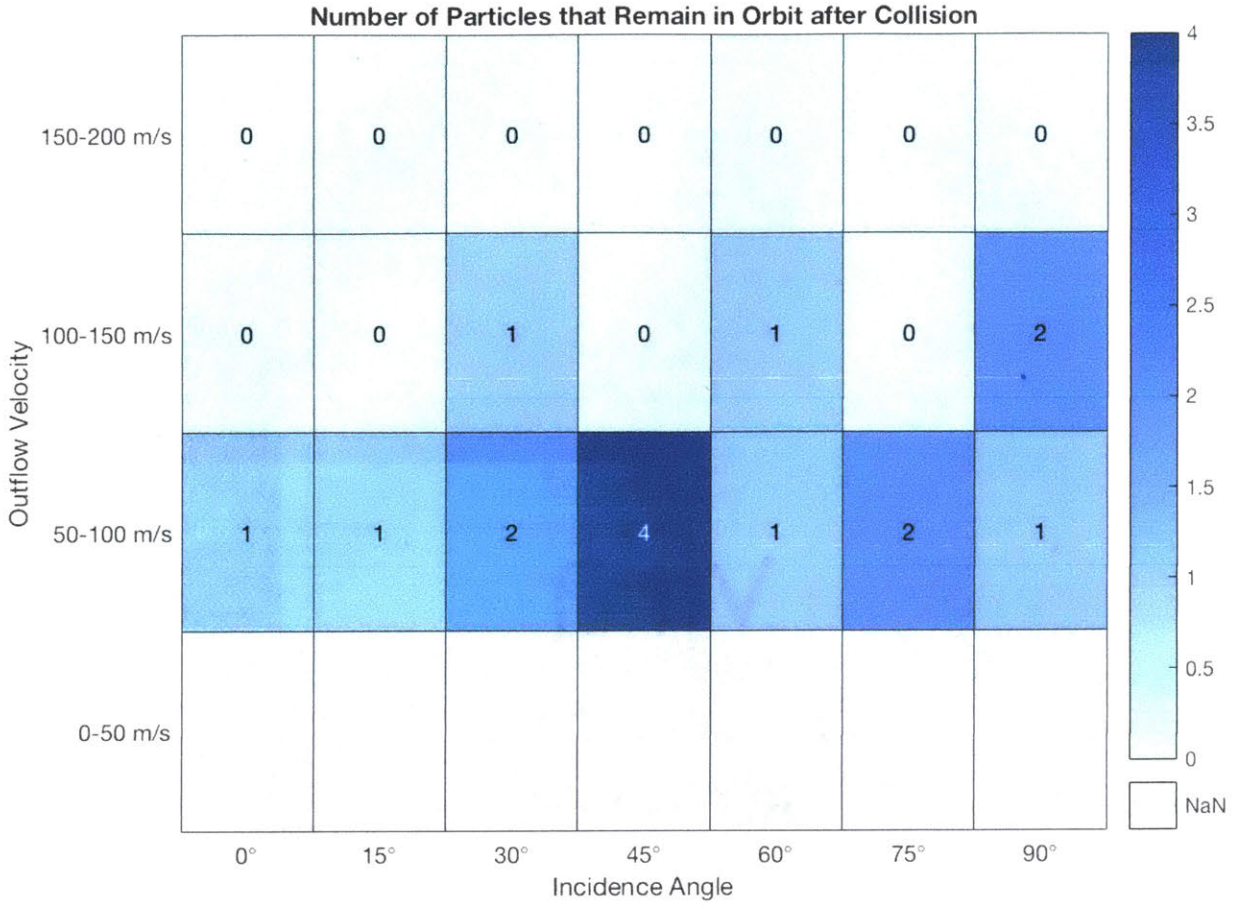

Figure 5. The number of outflow particles that remain in orbit around the body after colliding with the ring material. Because particles in the 0 m/s to 50 m/s velocity range do not reach the ring, no collisions occur, and so the number of particles that remain in orbit after colliding with the ring cannot be given for these trials.

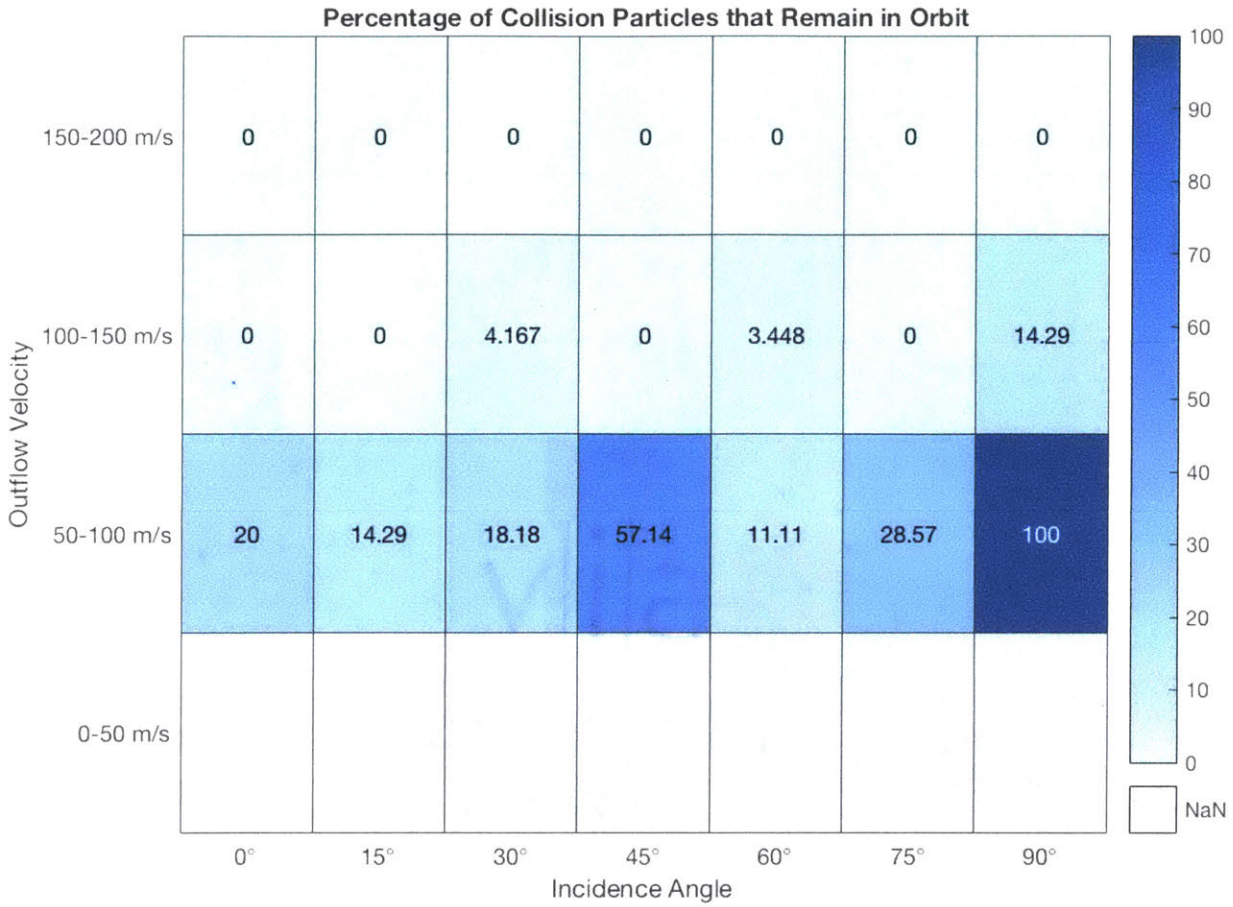

Figure 6. The percentage of outflow particles that remain in orbit around the body after colliding with the ring material. Because particles in the 0 m/s to 50 m/s velocity range do not reach the ring, no collisions occur, and so the percentage of particles that remain in orbit after colliding with the ring cannot be given for these trials.

In trials in which the outflow velocity was less than or equal to 100 m/s, approximately 90% or more of the particles fell back to the surface of the body (Figure 7). Nonetheless, 1% to 2% of particles fell back to the surface after colliding with the ring for five out of the eight trials with outflow velocities greater than 100 m/s and with incidence angles between 15° and 60°. The number of particles that escape exhibits the opposite pattern (Figure 8). For the trials in which the outflow velocity is greater than 100 m/s, 98% or more of the outflow particles escape. For trials in which the outflow velocity range is 50 m/s to 100 m/s, less than 10% of the particles escape, and these escaping particles are the particles that undergo collisions but do not stay in orbit.

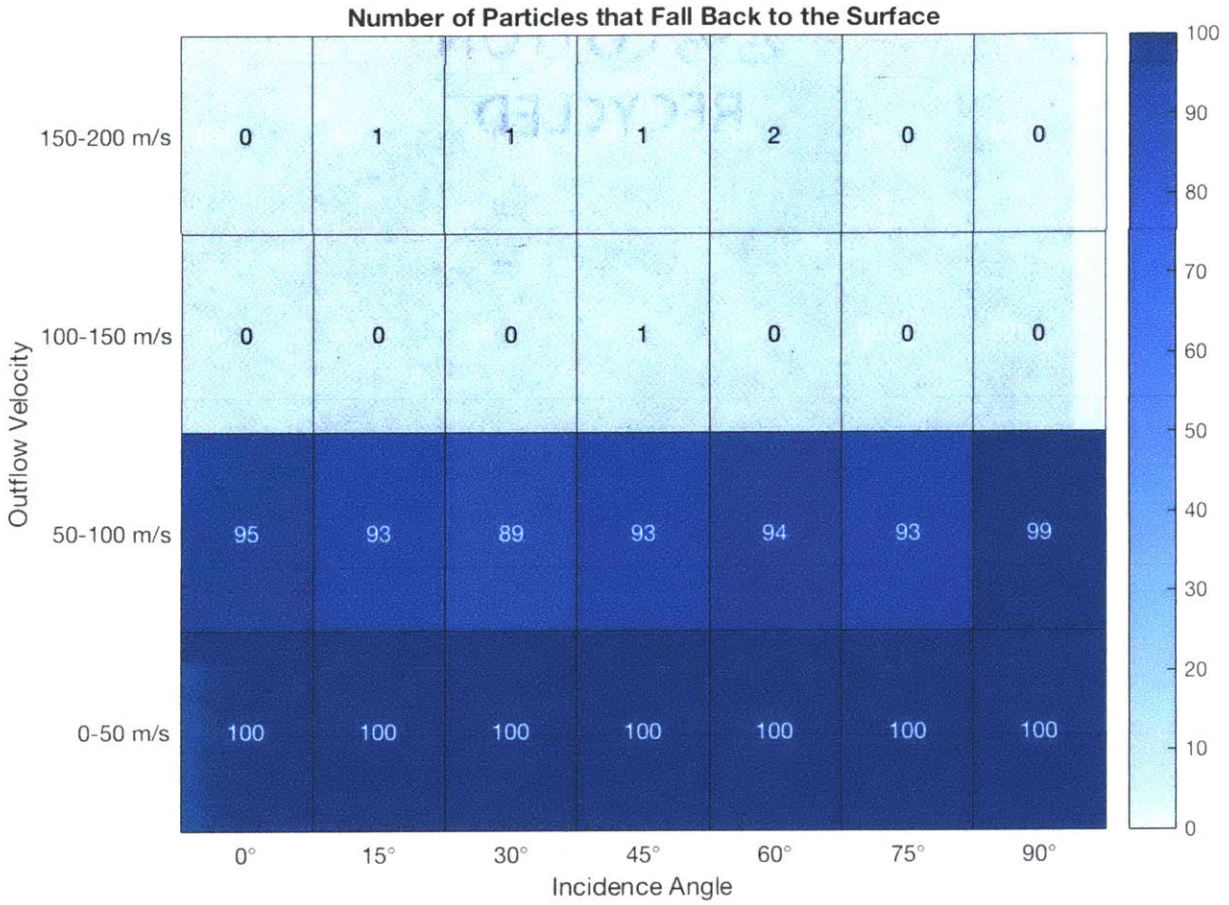

Figure 7. The number of outflow particles that fall back to the surface of the body. For each trial conducted with 100 total outflow particles, the number of outflow particles that fall back to the surface of the body is given.

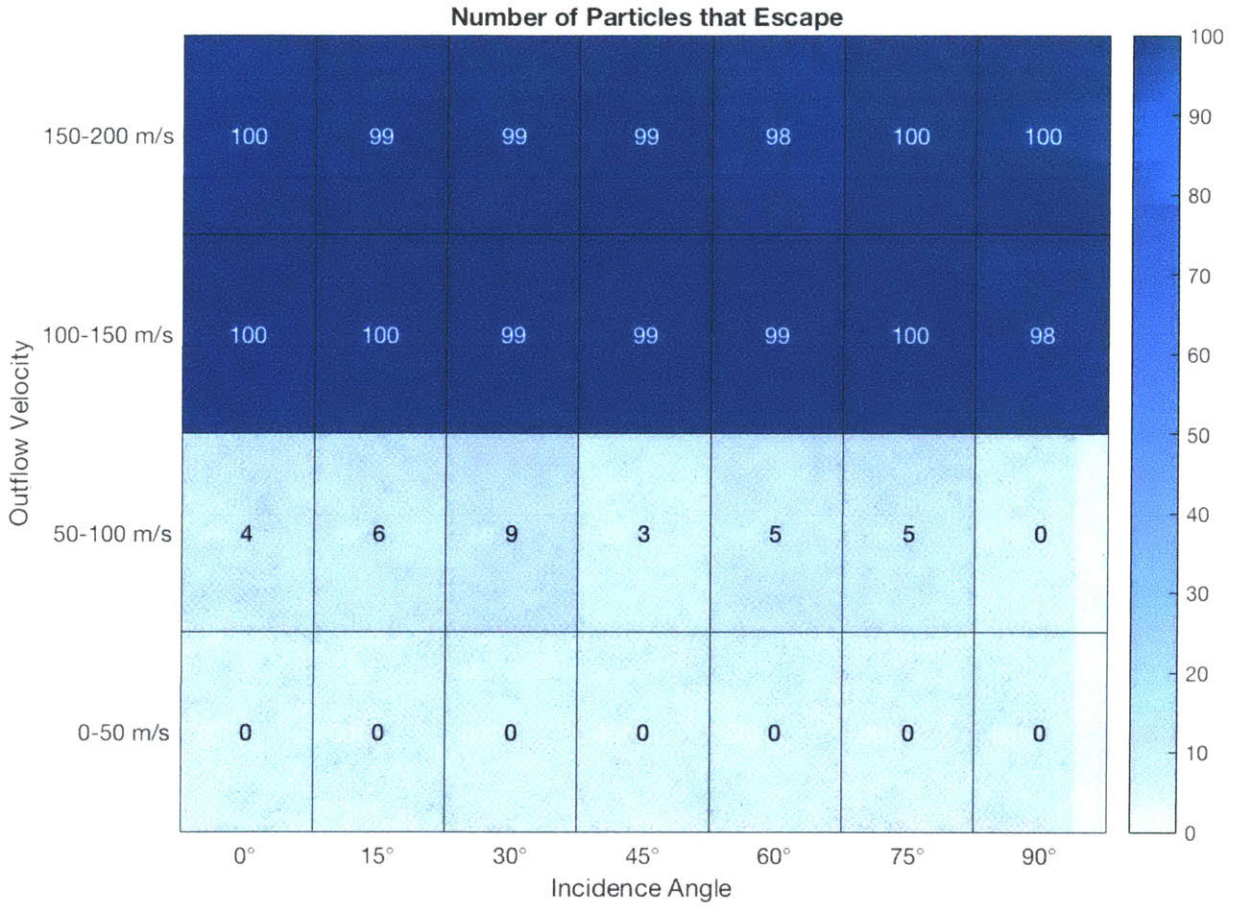

Figure 8. The number of outflow particles that escape. For each trial conducted with 100 total outflow particles, the number of outflow particles that escape is given.

Incidence angles greater than 75° result in an effective optical depth of the ring that is much less than the chosen edge-on value of $\tau_{ring} = 0.3$. For incidence angles less than 75°, the trends in these trials appear to be more strongly connected with the outflow velocity than with the incidence angle. Moreover, the outflow velocities that result in the largest number of outflow particles remaining in orbit appear to be velocities on the order of the escape velocity. However, outflows with velocities much larger than the escape velocity do not produce particles that stay in orbit around the small body, which poses a problem if the dust particles carried with the outflow are expected to be traveling at or close to the gas sound speed.

Several factors could cause the dust particles to travel at velocities that are less than the gas sound speed. The drag that a dust particle experiences can decrease its velocity such that its terminal velocity v_t can be expressed as

$$v_t = \frac{c_s}{1+f} \qquad (1)$$

in which c_s is the gas sound speed and f is the ratio between the mass of the dust and the mass of the gas (M. Pan, personal communication, December 31, 2017). If this mass ratio f is equal to 1, the terminal velocity of the dust can be reduce to half of the gas sound speed c_s. Although

collisions between outflow particles were not a focus in this second set of trials, such collisions could reduce the velocities of outflow particles before they reach and collide with the ring material. Lastly, the presence of overlying material could significantly slow outflow particles as they leave the surface of the body. A combination of these factors could further slow dust particles as they leave the body's surface.

Additionally, the orbiting particles do not orbit in the plane of the ring (Figure 9). Their orbits are not confined to the xy-plane, and because there is a z-component to their movement, they could undergo future collisions when passing through the ring material. Through these futures interactions, the particles could settle into the ring or escape. Thus, an outflow particle that remains in orbit around the body immediately following an outburst event does not necessarily remain in orbit over longer periods of time, though further collisions could cause the particle to join the ring. Longer integrations could provide insight into the fraction of particles retained in such a manner.

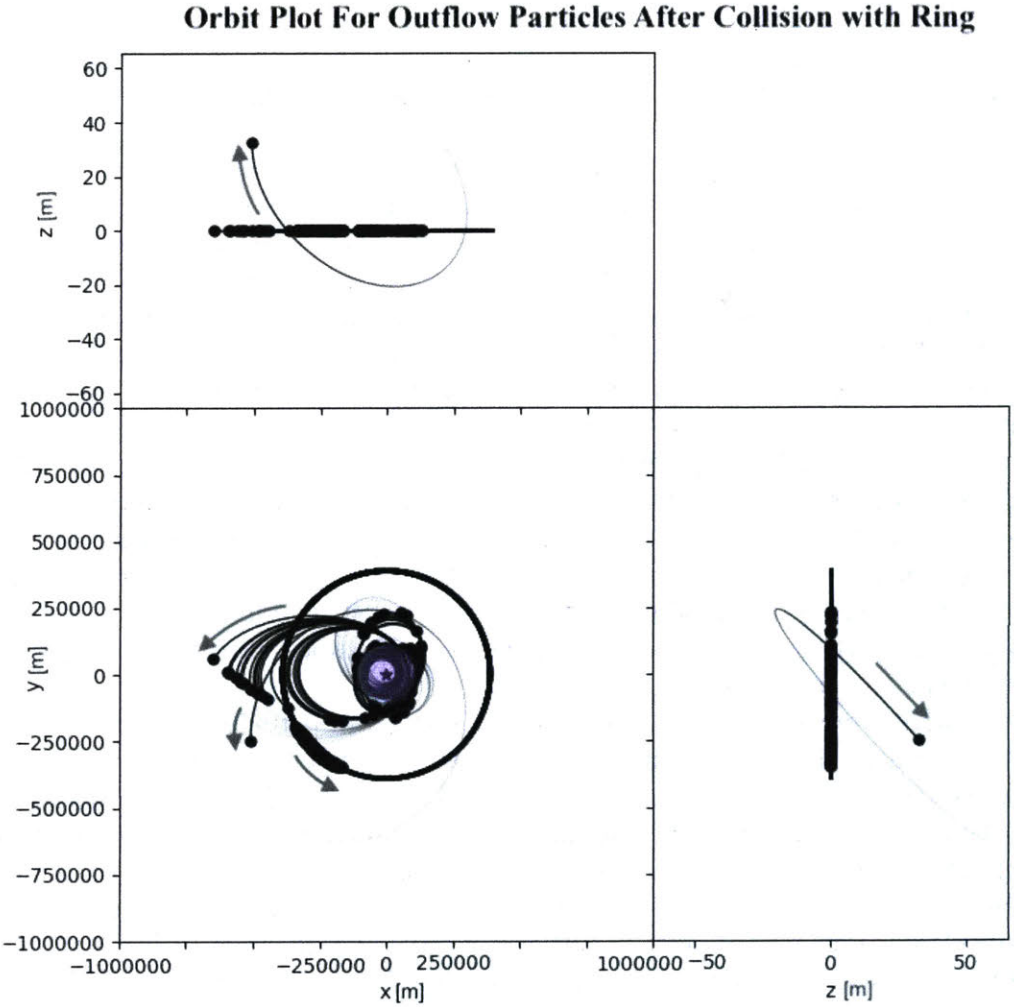

Figure 9. Orbit plot for outflow particles after collision with ring material, $\beta = 90°$ and v_i = 50 m/s to 100 m/s. The body is represented in the xy-plane in lavender. The arrows indicate the direction of motion of the particles. One collision occurred between the outflow particles and the ring material for this trial, and the particle that collided with the ring remains in orbit around the body. The other outflow particles continue to move in the

equatorial plane after passing through the ring region without colliding with any ring particles. The ring slice continues along its orbit in the equatorial plane after its initial setup in line with the outflow's trajectory.

Discussion

This study first examined Centaur ring formation stemming from mutual particle collisions within an outflow and then assessed Centaur ring replenishment in relation to particle collisions between an outflow and a pre-exiting structure. Based on the simple first set of trials in which collisions between outflow particles are made favorable through sporadic outbursts that release batches of particles at a fixed time interval, forming a ring around a Centaur from outflow material alone is difficult. For an outflow with an optical depth of $\tau_{outflow} = 0.3$, a mean of only 0.02% of the outflow particles remained in orbit around the body due to collisions with other outflow particles in the ten trials that were performed. Due to the large difference between the gas sound speed and the escape velocity for small bodies, the outflow particles are likely traveling too fast to remain in orbit, and the types of collisions that are required for them to remain in orbit are rare. Nevertheless, based on the 0.02% of particles in the outflow that remain in orbit about the body due to mutual collisions, sustained activity that lofts many particles over long periods of time could produce material that remains in orbit around the body, though the effects of radiation pressure would likely hamper this buildup of material. Thus, these trials still illustrate the challenges of forming a ring around a Centaur through outflow material alone.

The second set of trials demonstrates the possibility that outflow particles could contribute material to a ring structure that is already present around the body. Such a ring could form at any previous point in the Centaur's dynamical lifetime as a result of collisions, satellite disruption (Pan & Wu, 2016), three-body encounters (Melita et al., 2017), and giant planet encounters (Hyodo et al., 2016). For outflows traveling faster than the escape velocity, up to 34% of outburst particles can collide with the ring material, though this percentage is dependent on incidence angle. Incidence angles between 0° and 60° appear most favorable for the occurrence of collisions. For outflows traveling at velocities between that required to reach the ring and approximately 1.5 times the escape velocity, up to 1% to 4% of particles can remain in orbit around the body after colliding with the ring. Thus, although such rings are believed to be short-lived, with a collisional spreading time of 10^5 years (Pan & Wu, 2016) in comparison to a Centaur's lifetime of 10^6 years in the cis-Neptunian region, outburst activity could prolong the lifetime of a Centaur's ring system.

These trials were also limited in terms of the number of particles that could be added to each integration due to the difficulty of simulating a large number of particle collisions. This aspect affected the size chosen for the ring particles as well as the total number of particles that could be included in the outburst. The integration time for these trials was one rotation period of the Centaur, and while outflow particles were found to be in orbit around the body after collision with the ring material, their fate over longer timescales was not determined. Because retention was not considered, a fraction of outflow particles even smaller than 1% to 4% could be added to the ring. Even so, these trials demonstrate the possibility that outflow particles could contribute to pre-existing ring material.

A notable feature of the second set of trials was the number of outflow particles that fell back to the surface of the body. For outflows with velocities less than the escape velocity, the majority of particles returned to the body's surface as expected. However, for trials with outflow velocities greater than the escape velocity and with incidence angles from 15° to 60°, up to 1% to

2% of particles returned to the surface of the body after colliding with the ring material. The population of active Centaurs is overall bluer or more neutral in color than the redder population of inactive Centaurs, and this aspect has been attributed to a surface freshening process associated with activity (Jewitt, 2015). The amount of fallback in these trials could lend support to the idea that activity can refresh a Centaur's surface.

Conclusions and Future Work

Centaur surface activity can deliver material into orbit around the body, feasibly replenishing a pre-existing ring structure. This process could help to maintain such ring structures over time scales longer than 10^5 years and potentially over the lifetime of a Centaur in the cis-Neptunian region.

Future work should repeat the trials performed in this study, as only one run of each was completed, rendering the results subject to small number statistics. Running these trials with more particles would also improve the statistics with regard to the results. Future trials could also carry out longer integrations to determine whether outflow particles in orbit around the body undergo more collisions with the ring material or settle into the ring structure.

Additionally, future trials could also address several factors not explored in this study. Trials could be conducted with the influence of radiation pressure to measure its effects on the fate of the ring particles. Different outflow morphologies could be explored in order to assess the affects of mutual collisions between outflow particles in combination with collisions between outflow particles and material already present around the body. Perhaps more continuous yet variable outbursts, such as activity that built up and trailed off over time, would be more realistic and would produce more interactions between outflow particles. Interactions between outflow particles and other particle structures such as a coma could also be simulated. These future studies could provide greater insight into the mechanisms of activity that are present in Centaurs with observed particle structures.

References

Barkume, K. M., Brown, M. E., & Schaller, E. L. (2008). Near-infrared spectra of Centaurs and Kuiper belt objects. *The Astronomical Journal, 135*(1), 55-67. http://doi.org/10.1088/0004-6256/135/1/55.

Braga-Ribas, F., Sicardy, B., Ortiz, J. L., Snodgrass, C., Roques, F., Vieira-Martins, R., Camargo, J. I. B., Assafin, M., Duffard, R., Jehin, E., Pollock, J., Leiva, R., Emilio, M., Machado, D. I., Colazo, C., Lellouch, E., Skottfelt, J., Gillon, M., Ligier, N., Maquet, L., Benedetti-Rossi, G., Gomes, A. Ramos, Kervella, P., Monteiro, H., Sfair, R., El Moutamid, M., Tancredi, G., Spagnotto, J., Maury, A., Morales, N., Gil-Hutton, R., Roland, S., Ceretta, A., Gu, S.-H., Wang, X.-B., Harpsøe, K., Rabus, M., Manfroid, J., Opitom, C., Vanzi, L., Mehret, L., Lorenzini, L., Schneiter, E. M., Melia, R., Lecacheux, J., Colas, F., Vachier, F., Widemann, T., Almenares, L., Sandness, R. G., Char, F., Perez, V., Lemos, P., Martinez, N., Jørgensen, U. G., Dominik, M., Roig, F., Reichart, D. E., Lacluyze, A. P., Haislip, J. B., Ivarsen, K. M., Moore, J. P., Frank, N. R., & Lambas, D. G. (2014). A ring system detected around the Centaur (10199) Chariklo. *Nature, 508*(7494), 72-75. http://doi.org/10.1038/nature13155.

Brown, W. R. & Luu, J. X. (1998). Properties of model comae around Kuiper belt and Centaur objects. *Icarus, 135*(2), 415-430. http://doi.org/10.1006/icar.1998.5964.

Bus, S. J., A'Hearn, M. F., Schleicher, D. G., & Bowell, E. (1991). Detection of CN emission from (2060) Chiron. *Science, 251*(4995), 774-777. http://doi.org/10.1126/science.251.4995.774.

Charnoz, S., Canup, R. M., Crida, A., & Dones, L. (2017). The origin of planetary ring systems. In M. S. Tiscareno & C. D. Murray (Eds.), *Planetary Ring Systems: Properties, Structure, and Evolution.* Pending publication.

Choi, Y.-J., Weissman, P. R., & Polishook, D. (2006). (60558) 2000 EC_98. In Green, D. W. E. (Ed.), *IAU Circ., 8656*(2). Retrieved from http://www.cbat.eps.harvard.edu/iauc/08600/08656.html#Item2.

de Pater, I. & Lissauer, J. J. (2015). Magnetic fields and plasmas. In *Planetary Sciences* (2nd ed.). Cambridge: Cambridge University Press.

Dones, L., Levison H. F., & Duncan, M. (1996). On the dynamical lifetimes of planet-crossing objects. In T. W. Rettig & J. M. Hahn (Eds.), *Astronomical Society of the Pacific Conference Series: Completing the Inventory of the Solar System, Volume 107* (233-244). San Francisco: Astronomical Society of the Pacific.

Duffard, R., Pinilla-Alonso, N., Ortiz, J. L., Alvarez-Candal, A., Sicardy, B., Santos-Sanz, P., Morales, N., Colazo, C., Fernández-Valenzuela, E., & Braga-Ribas, F. (2014). Photometric and spectroscopic evidence for a dense ring system around Centaur

Chariklo. *Astronomy & Astrophysics*, *568*(A79). http://doi.org/10.1051/0004-6361/201424208.

Finson, M. J. & Probstein, R. F. (1968). A theory of dust comets- I. Model and equations. *The Astrophysical Journal*, *154*, 327-352. http://doi.org/10.1086/149761.

Foster, M. J., Green, S. F., McBride, N., & Davies, J. K. (1999). Note: Detection of water ice on 2060 Chiron. *Icarus*, *141*(2), 408-410. http://doi.org/10.1006/icar.1999.6180

Fornasier, S., Lellouch, E., Müller, T., Santos-Sanz, P., Panuzzo, P., Kiss, C., Lim, T., Mommert, M., Bockelée-Morvan, D., Vilenius, E., Stansberry, J., Tozzi, G. P., Mottola, S., Delsanti, A., Crovisier, J., Duffard, R., Henry, F., Lacerda, P., Barucci, A., & Gicquel, A. (2013). TNOs are Cool: A survey of the trans-Neptunian region- VIII. Combined Herschel PACS and SPIRE observations of nine bright targets at 70-500 μm. *Astronomy & Astrophysics*, 555(A15).

Gehrels, T. (1999). A review of comet and asteroid statistics. *Earth, Planets and Space*, *51*, 1155-1161. http://doi.org/10.1186/BF03351590.

Horner, J., Evans, N. W., Bailey, M. E., & Asher, D. J. (2003). The populations of comet-like bodies in the Solar system. *Monthly Notices of the Royal Astronomical Society*, *343*, 1057-1066. http://doi.org/10.1046/j.1365-8711.2003.06714.x.

Horner, J., Evans, N. W., & Bailey, M. E. (2004). Simulations of the population of Centaurs- I. The bulk statistics. *Monthly Notices of the Royal Astronomical Society*, *354*, 798-810. http://doi.org/10.1111/j.1365-2966.2004.08240.x.

Hyodo, R., Charnoz, S., Genda, H., & Ohtsuki, K. (2016). Formation of Centaurs' rings through their partial tidal disruption during planetary encounters. *The Astrophysical Journal Letters*, *828*(1:L8). http://doi.org/10.3847/2041-8205/828/1/L8.

Jet Propulsion Laboratory. (n.d.) JPL Small-Body Database Browser: 2060 Chiron (1977 UB). Retrieved from https://ssd.jpl.nasa.gov/sbdb.cgi#top.

Jewitt, D. (2009). The active Centaurs. *The Astronomical Journal*, *137*, 4296-4312. http://doi.org/10.1088/0004-6256/137/5/4296.

Jewitt, D. (2015). Color systematics of comets and related bodies. *The Astronomical Journal*, *150*(6:A201). http://doi.org/10.1088/0004-6256/150/6/201.

Luu, J. X. & Jewitt, D. (1996). Color diversity among the Centaurs and Kuiper belt objects. *The Astronomical Journal*, *112*(5), 2310-2318. http://doi.org/10.1086/118184.

Luu, J. X. & Jewitt, D. (1990). Cometary activity in 2060 Chiron. *The Astronomical Journal*, *100*, 913-932. http://doi.org/10.1086/115571

Meech, K. J. & Belton, M. J. S. (1989). (2060) Chiron. In Green, D. W. E. (Ed.), *IAU Circ.*, *4770*(1). Retrieved from http://www.cbat.eps.harvard.edu/iauc/04700/04770.html#Item1.

Melita, M. D., Duffard, R., Ortiz, J. L., & Campo-Bagatin, A. (2017). Assessment of different formation scenarios for the ring system of (10199) Chariklo. *Astronomy & Astrophysics*, 602(A27). http://doi.org/10.1051/0004-6361/201629858.

Ortiz, J. L., Duffard, R., Pinilla-Alonso, N., Alvarez-Candal, A., Santos-Sanz, P., Morales, N., Fernández-Valenzuela, E., Licandro, J., Campo Bagatin, A., & Thirouin, A. (2015). Possible ring material around centaur (2060) Chiron. *Astronomy & Astrophysics*, *576*(A18). http://doi.org/10.1051/0004-6361/201424461.

Ortiz, J. L., Santos-Sanz, P., Sicardy, B., Benedetti-Rossi, G., Bérard, D., Morales, N., Duffard, R., Braga-Ribas, F., Hopp, U., Ries, C., Nascimbeni, V., Marzari, F., Granata, V., Pál, A., Kiss, C., Pribulla, T., Komžík, R., Hornoch, K., Pravec, P., Bacci, P., Maestripieri, M., Nerli, L., Mazzei, L., Bachini, M., Martinelli, F., Succi, G., Ciabattari, F., Mikuz, H., Carbognani, A., Gaehrken, B., Mottola, S., Hellmich, S., Rommel, F. L., Fernández-Valenzuela, E., Bagatin, A. Campo, Cikota, S., Cikota, A., Lecacheux, J., Vieira-Martins, R., Camargo, J. I. B., Assafin, M., Colas, F., Behrend, R., Desmars, J., Meza, E., Alvarez-Candal, A., Beisker, W., Gomes-Junior, A. R., Morgado, B. E., Roques, F., Vachier, F., Berthier, J., Mueller, T. G., Madiedo, J. M., Unsalan, O., Sonbas, E., Karaman, N., Erece, O., Koseoglu, D. T., Ozisik, T., Kalkan, S., Guney, Y., Niaei, M. S., Satir, O., Yesilyaprak, C., Puskullu, C., Kabas, A., Demircan, O., Alikakos, J., Charmandaris, V., Leto, G., Ohlert, J., Christille, J. M., Szakáts, R., Farkas, A. Takácsné, Varga-Verebélyi, E., Marton, G., Marciniak, A., Bartczak, P., Santana-Ros, T., Butkiewicz-Bąk, M., Dudziński, G., Alí-Lagoa, V., Gazeas, K., Tzouganatos, L., Paschalis, N., Tsamis, V., Sánchez-Lavega, A., Pérez-Hoyos, S., Hueso, R., Guirado, J. C., Peris, V., & Iglesias-Marzoa, R. (2017). The size, shape, density and ring of the dwarf planet Haumea from a stellar occultation. *Nature*, *550*(7675), 219-223. http://doi.org/10.1038/nature24051.

Pan, M., & Wu, Y. (2016). On the mass and origin of Chariklo's rings. *The Astrophysical Journal*, *821*(1:18). http://doi.org/10.3847/0004-637X/821/1/18.

Parker, J. W. M., Stern, A. S., Festou, M. C., A'Hearn, M. F., & Weintraub, D. A. (1997). Ultraviolet observations of Chiron with the HST/FOS: Examining a Centaur's gray matter. *The Astronomical Journal*, *113*(5), 1899-1908. http://doi.org/10.1086/118403.

Rein, H. & Liu, S.-F. (2012). REBOUND: an open-source multi-purpose N-body code for collisional dynamics. *Astronomy & Astrophysics*, *537*(A128). http://doi.org/10.1051/0004-6361/201118085.

Rein, H., Liu, S., Spiegel, D. S., Fujii, A., & Tamayo, D. (2015). *Integrating eccentric comets with MERCURIUS (iPython)*. Retrieved from http://rebound.readthedocs.io/en/latest/ipython/EccentricComets.html.

Rein, H., Liu, S., Spiegel, D. S., Fujii, A., & Tamayo, D. (2015). *Simulating Saturn's rings (iPython)*. Retrieved from http://rebound.readthedocs.io/en/latest/ipython/SaturnsRings.html.

Romanishin, W., Tegler, S. C., Levine, J., & Butler, N. (1997). BVR Photometry of Centaur Objects 1995 GO, 1993 HA2, and 5145 Pholus. *The Astronomical Journal, 113*(5), 1893-1898. http://doi.org/10.1086/118402.

Ruprecht, J. D., Bosh, A. S., Person, M. J., Bianco, F. B., Fulton, B. J., Gulbis, A. A. S., Bus, S. J., & Zangari, A. M. (2015). 29 November 2011 stellar occultation by 2060 Chiron: Symmetric jet-like features. *Icarus, 252*, 271-276. http://doi.org/10.1016/j.icarus.2015.01.015.

Williams, D. R. (2014). *Chiron Fact Sheet*. Retrieved from http://nssdc.gsfc.nasa.gov/planetary/factsheet/chironfact.html.

Womack, M. & Stern S. A. (1997). Observations of carbon monoxide in (2060) Chiron. *28th Annual Lunar and Planetary Science Conference*, 575.

Appendix A

The escape velocity for a body with the mass and radius of Chiron was calculated using

$$v_{esc} = \sqrt{\frac{2GM}{r}} = \sqrt{\frac{2*6.6741*10^{-11}\left[\frac{m^3}{kg*s^2}\right]*10^{19}[kg]}{109*10^3[m]}} = 110.7\ \frac{m}{s} \quad \text{(A1)}$$

in which M is the mass of Chiron (Williams, 2014), r is the radius of Chiron (Fornasier et al., 2013), and G is the universal gravitational constant.

The gas sound speed was calculated using

$$c_S = \sqrt{\frac{\gamma P}{\rho}} = \sqrt{\frac{\gamma kT}{\mu_a m_{amu}}} = \sqrt{\frac{\frac{5}{3}*1.3806*10^{-23}\left[\frac{m^2kg}{s^2K}\right]*91.8[K]}{1.0079\,[amu]*1.6605*10^{-27}\left[\frac{kg}{amu}\right]}} = 1123.4\ \frac{m}{s} \quad \text{(A2)}$$

(de Pater & Lissauer, 2015) in which γ is the ratio of specific heats, T is the temperature of the medium, ρ is the density of the medium, and k is the Boltzmann constant. The temperature was found by calculating the black body temperature at Chiron's perihelion distance using

$$T_{BB} = \left(\frac{(1-A)L_{Sun}}{16\pi a^2\sigma_{SB}}\right)^{\frac{1}{4}} = \left(\frac{(1-0.16)*3.828*10^{26}[W]}{16\pi*(1.2613*10^{12}[m])^2*5.6704*10^{-8}\left[\frac{W}{m^2K^4}\right]}\right)^{\frac{1}{4}} = 91.8\ K \quad \text{(A3)}$$

(Pan & Wu, 2016) in which A is the body's albedo (Fornasier et al., 2013), L_{sun} is the solar luminosity, σ_{SB} is the Stefan-Boltzmann constant, and a is the semi-major axis of the body, although Chiron's perihelion distance q = 8.4311 AU was used rather than the semi-major axis a = 13.6482 (Jet Propulsion Laboratory Small-Body Database Browser, n.d.) due to the increase in the likelihood of activity with decreasing distance from the sun.

The magnitude of the rotational velocity of a particle ejected at the body's equator was calculated using

$$v_{rot} = \omega r = \frac{2\pi r}{P} = \frac{2\pi*(109*10^3[m])}{21305[s]} = 32.1\ \frac{m}{s} \quad \text{(A4)}$$

in which P is the rotation period of Chiron (Jet Propulsion Laboratory Small-Body Database Browser, n.d.) and r is the radius of Chiron (Fornasier et al., 2013).

Appendix B

This appendix contains the Python code used for the outflow particle collision trials in REBOUND. The code for the simulation is as follows.

```
import rebound
import numpy as np
import matplotlib
import matplotlib.pyplot as plt
import math
import random
from random import randint
from random import uniform

sim = rebound.Simulation()

#define SI units
sim.units = ('s','m','kg')

#integrator options
sim.integrator = "hermes"
sim.testparticle_type = 1

#collision and boundary options
sim.collision = "direct"
sim.collision_resolve = "hardsphere"
sim.collision_resolve_keep_sorted = 1
sim.boundary = "open"
boxsize = 1e10
sim.configure_box(boxsize)
sim.track_energy_offset = 1

sim.move_to_com()

#adding centaur characteristics
r_body=109e3              #radius of the body [m]
m_body=1e19               #mass of the body [kg]
rotperh=5.918             #rotation period of the body [h]
rotpers=3600*rotperh      #rotation period of the body [s]

#simulation times, all in seconds
sim.t=0                   #starting the simulation at t = 0 s
tmax = 100                #ending the simulation at t = 100 s
sim.dt = 1                #using timestep of 1 s

#adding centaur
sim.add(m=m_body, r=r_body, hash="Centaur")
print("Centaur added.\n")
```

```
#adding initial particles
N_testparticle = 100     #number of particles in first burst
m=4.19e3                 #[kg]
r=1                      #[m]

for particle in range(1,N_testparticle+1):
     #particle positions chosen from within swath at equator,
     #swath area corresponds to desired optical depth of 0.3

     alpha=uniform((math.pi/6.)-0.006,(math.pi/6.)+0.006)
     x=r_body*math.cos(alpha)
     y=r_body*math.sin(alpha)
     z=0

     if x!=0:
          angle_vel=((2*np.pi)/rotpers)*r_body
          vx_rotation=-angle_vel*np.sin(alpha)
          vy_rotation=angle_vel*np.cos(alpha)

          #watch out for the signs of the components, as they
          #depend on the quadrant of the angle alpha

     #x and y components of velocity chosen randomly
     #from given range
     vx=randint(0,200)
     vy=randint(0,200)
     vz=0

     p=sim.add(m=m, r=r, x=x, y=y, z=z, vx=vx+vx_rotation,
     vy=vy+vy_rotation, vz=vz)

#printing particle initials
for n in reversed(range(1,N_testparticle+1)):
     p=sim.particles[n]
     print(sim.t, p.x, p.y, p.z, p.vx, p.vy, p.vz, p.e, p.a,
     p.a*(1-p.e))

print("\nInitial particles added. Initial t, x, y, z, vx, vy,
vz, e, a, a(1-e) given above for each particle.\n")

sim.N_active = sim.N

print("Number of active particles = {} \n".format(sim.N_active))

#integration and plots
integ_steps = 11
new_batch=100
```

```
integ_times = np.linspace(0, tmax, integ_steps)
for i, sim_time in enumerate(integ_times):
     sim.integrate(sim_time)
     for n in range(1,N_testparticle):
          p = sim.particles[n]
          print('%15.5f   %15.5f   %15.5f    %15.5f    %15.5f
          %15.5f   %15.5f   %15.5f   %15.5f   %15.5f   %15.5f'
          %(sim.t, p.x, p.y, p.z, p.vx, p.vy, p.vz, p.e, p.a,
          (p.a*(1-p.e)), p.lastcollision))
     sim.N_active=sim.N
     print("\nNumber of active particles = {}
     \n".format(sim.N_active))

     for newparticle in range(1,new_batch+1):
          alpha=uniform((math.pi/6.)-0.006,(math.pi/6.)+0.006)
          x=r_body*math.cos(alpha)
          y=r_body*math.sin(alpha)
          z=0

          if x!=0:
               angle_vel=((2*np.pi)/rotpers)*r_body
               vx_rotation=-angle_vel*np.sin(alpha)
               vy_rotation=angle_vel*np.cos(alpha)

          vx=randint(0,200)
          vy=randint(0,200)
          vz=0
          p=sim.add(m=m, r=r, x=x, y=y, z=z, vx=vx+vx_rotation,
          vy=vy+vy_rotation, vz=vz)
     for n in
     reversed(range(N_testparticle,N_testparticle+new_batch+1)):
          p=sim.particles[n]
     N_testparticle=N_testparticle+new_batch
     print("{} new particles added for next
integration.".format(new_batch))
     print("{} particles now exist.\n".format(N_testparticle))

for n in range(1,N_testparticle+1):
     p = sim.particles[n]
     print('%15.5f   %15.5f   %15.5f    %15.5f    %15.5f
     %15.5f   %15.5f   %15.5f   %15.5f   %15.5f   %15.5f'
     %(sim.t, p.x, p.y, p.z, p.vx, p.vy, p.vz, p.e, p.a,
     (p.a*(1-p.e)), p.lastcollision))
     print("Integrated for all steps. t, x, y, z, vx, vy, vz, e,
     a, a(1-e) given above for each particle.\n")

orbitfig=rebound.OrbitPlot(sim, trails=True, slices=True)
plt.show(orbitfig)
```

Appendix C

This appendix contains the Python code used for the ring collision trials in REBOUND. This code was originally based on the "Integrating eccentric comets with MERCURIUS (iPython)" example found in the online REBOUND documentation (Rein, Liu, Spiegel, Fujii, & Tamayo, 2015).

The Python code for the simulation is as follows.

```
import rebound
import numpy as np
import matplotlib
import matplotlib.pyplot as plt
import math
import random
from random import randint
from random import uniform

sim = rebound.Simulation()

#specify SI units
sim.units = ('s','m','kg')

#integrator options
sim.integrator = "hermes"

#collision and boundary options
sim.collision = "direct"
sim.collision_resolve = "hardsphere"
sim.collision_resolve_keep_sorted = 1
sim.boundary = "open"
boxsize = 109e3*1000
sim.configure_box(boxsize)
sim.track_energy_offset = 1

sim.move_to_com()

############################################################

#adding centaur characteristics
r_body=109e3              #radius of the body [m]
m_body=1e19               #mass of body [kg]
rotperh=5.918             #rotation period of the body [h]
rotpers=3600*rotperh      #rotation period of the body [s]

#adding centaur
sim.add(m=m_body, r=r_body, hash="Centaur")
print("Centaur added.\n")
```

```
#################################################################

#simulation times, all in seconds
sim.t=0              #begin simulation at t = 0 s
tmax = rotpers       #integrate for one rot. per. of the body
sim.dt = 1           #using timestep of 1 s

#################################################################

#defining angles involved in both ring particle and outburst
particle initials
alpha=math.pi/6.
beta=math.pi/2.          #***vary me!***

#################################################################

#adding ring particles
Rring_center=390e3              #[m]
Ring_width=6e3                  #[m]
Rring_inner=Rring_center-Ring_width
Rring_outer=Rring_center+Ring_width
opticaldepth=0.3
sliceangle=(alpha)

rringparticles= 100      #[m]
rhoringparticles= 1000   #[kg/m^3]
mringparticles=(4./3.)*math.pi*rringparticles**3*(rhoringparticl
es)                      #[kg]

slicenumber=(sliceangle/(2*math.pi))*opticaldepth*(2*math.pi*Rri
ng_center)/(rringparticles*2)
N_ringparticle = int(slicenumber)

print("\nThere will be %d ring particles.\n" %N_ringparticle)

np.random.seed(37)

for particle in range(1,N_ringparticle+1):
     sim.testparticle_type = 1
     a=uniform(Rring_inner,Rring_outer)
     e=0
     f=uniform(beta-sliceangle,beta)
     ringparticle=sim.add(m=mringparticles, r=rringparticles,
     a=a, e=e, f=f, hash="ring")

#printing ring particle initials
for n in reversed(range(1,N_ringparticle+1)):
     p=sim.particles[n]
```

```
        print(sim.t, p.x, p.y, p.z, p.vx, p.vy, p.vz, p.e, p.a,
        p.a*(1-p.e), p.P)

print("\nAll ring particles added. Initial t, x, y, z, vx, vy,
vz, e, a, a(1-e), P given above for each particle.\n")

sim.N_active = sim.N

#################################################################

#adding outburst particles
N_outburstparticle = 100

vesc=((1/r_body)*2*6.67408e-11*m_body)**0.5  #[m/s]

for particle in range(1,N_outburstparticle+1):

        mout=4.19e-15  #[kg]
        rout=1e-6      #[m]

        sim.testparticle_type = 1

        R=r_body
        x=R*math.cos(alpha)
        y=R*math.sin(alpha)
        z=uniform(-0.0001,0.0001) #It gets mad if z=0.
                                  #Don't ask me why.

        if x!=0:
                v_rot=((2*math.pi)/rotpers)*(x**2+y**2)**0.5 #[m/s]
                vx_rotation=-v_rot*np.sin(alpha)             #[m/s]
                vy_rotation=v_rot*np.cos(alpha)              #[m/s]

                v_shoot=uniform(0,50)    #***vary me!***     #[m/s]
                vx=v_shoot*np.cos(alpha+beta)                #[m/s]
                vy=v_shoot*np.sin(alpha+beta)                #[m/s]
                vz=0

        outburstparticle=sim.add(m=mout, r=rout, x=x, y=y, z=z,
        vx=vx+vx_rotation, vy=vy+vy_rotation, vz=vz)

sim.N_active = sim.N

#printing outburst particle initials
for n in range(1,N_outburstparticle+1):
        p=sim.particles[n]
        print(sim.t, p.x, p.y, p.z, p.vx, p.vy, p.vz, p.e, p.a,
        p.a*(1-p.e))
```

```
print("\nAll outburst particles added. Initial t, x, y, z, vx,
vy, vz, e, a, a(1-e) given above for each particle.\n")

############################################################

#integration and plots
#orbit plots generated and saved at each step
N_particles=N_ringparticle+N_outburstparticle
integ_steps = 10
data_array = np.zeros((integ_steps, 3, N_particles))
integ_times = np.linspace(0, tmax, integ_steps)
for i, sim_time in enumerate(integ_times):
     sim.integrate(sim_time)
     for n in range(1,N_particles):
          p = sim.particles[n]
          print(sim.t, p.x, p.y, p.z, p.vx, p.vy, p.vz, p.e,
          p.a, p.a*(1-p.e), p.lastcollision)
          data_array[i,0,n-1]=p.x
          data_array[i,1,n-1]=p.y
          data_array[i,2,n-1]=p.z
     fig= rebound.OrbitPlot(sim, lim=1e6, trails=True,
     slices=True)
     plt.savefig("orbit" + str(i) + ".png")
     print("\nStep %d completed.\n" %i)

print("\nIntegrated for all steps. t, x, y, z, vx, vy, vz, e, a,
a(1-e) given above for each particle.\n")

#rainbow dot plots and line plots created at end
for j in range(0,N_particles):
     xpoints=data_array[:,0,j]
     ypoints=data_array[:,1,j]
     plt.figure(integ_steps+1)
     plt.scatter(xpoints,ypoints,marker=".",linewidth='0');
     plt.xlim(-1e6,1e6)
     plt.ylim(-1e6,1e6)
     plt.savefig("xydot.png")

print("\nDot plot completed.\n")

for j in range(0,N_particles):
     xpoints=data_array[:,0,j]
     ypoints=data_array[:,1,j]
     plt.figure(integ_steps+2)
     plt.plot(xpoints,ypoints,linewidth='1');
     plt.xlim(-1e6,1e6)
     plt.ylim(-1e6,1e6)
```

```
     plt.savefig("xyline.png")

print("\nFirst line plot completed.\n")

for j in range(0,N_particles):
     xpoints=data_array[:,0,j]
     zpoints=data_array[:,2,j]
     plt.figure(integ_steps+3)
     plt.plot(xpoints,zpoints,linewidth='1');
     plt.xlim(-1e6,1e6)
     plt.ylim(-1e6,1e6)
     plt.savefig("xzline.png")

print("\nSecond line plot completed.\n")

for j in range(0,N_particles):
     ypoints=data_array[:,1,j]
     zpoints=data_array[:,2,j]
     plt.figure(integ_steps+4)
     plt.plot(ypoints,zpoints,linewidth='1');
     plt.xlim(-1e6,1e6)
     plt.ylim(-1e6,1e6)
     plt.savefig("yzline.png")

print("\nThird line plot completed.\n")

#print things for particles that have collided
print("\nParticles that have collided:\n")
for n in range(1,N_particles):
     p = sim.particles[n]
     if p.lastcollision>0:     #this will include ring particles
                               #that underwent collisions
          print(sim.t, p.x, p.y, p.z, p.vx, p.vy, p.vz, p.e,
          p.a, p.a*(1-p.e), p.lastcollision)

#print things for particles that have fallen back
print("\nParticles that have fallen back to surface:\n")
for n in range(1,N_particles):
     p = sim.particles[n]
     if p.a*(1-p.e)<r_body:
          print(sim.t, p.x, p.y, p.z, p.vx, p.vy, p.vz, p.e,
          p.a, p.a*(1-p.e), p.lastcollision)

#print array
print(data_array)

print("\nAll done.\n")
```

Appendix D

This appendix contains the Python code used for the shearing sheet trials in REBOUND. This code was taken from the "Simulating Saturn's rings (iPython)" example found in the online REBOUND documentation (Rein, Liu, Spiegel, Fujii, & Tamayo, 2015).

This example requires the user to calculate the epicyclic frequency, which is named "OMEGA" in the code. This value can be calculated using

$$\Omega = \sqrt{\frac{GM}{a^3}} = \sqrt{\frac{6.6741*10^{-11}\left[\frac{m^3}{kg*s^2}\right]*10^{19}\,[kg]}{(390*10^3\,[m])^3}} = 0.000106072 \qquad \text{(D1)}$$

in which M is the mass of the body, a is the orbital radius of the ring, and G is the universal gravitational constant.

The Python code for the simulation is as follows.

```
import rebound
import numpy as np
sim = rebound.Simulation()

OMEGA = 0.000106072     # [1/s]

sim.ri_sei.OMEGA = OMEGA

surface_density = 1000.    # kg/m^2
particle_density = 1000.   # kg/m^3

sim.G = 6.67428e-11        # N m^2 / kg^2

sim.dt = 1e-3*2.*np.pi/OMEGA

sim.softening = 0.2        # [m]

boxsize = 200.             # [m]
sim.configure_box(boxsize)
sim.configure_ghostboxes(2,2,0)

sim.integrator = "sei"
sim.boundary   = "shear"
sim.gravity    = "tree"
sim.collision  = "tree"

def cor_bridges(r, v):
        eps = 0.32*pow(abs(v)*100.,-0.234)
        if eps>1.:
            eps=1.
        if eps<0.:
            eps=0.
```

```
        return eps
sim.coefficient_of_restitution = cor_bridges

def powerlaw(slope, min_v, max_v):
    y = np.random.uniform()
    pow_max = pow(max_v, slope+1.)
    pow_min = pow(min_v, slope+1.)
    return pow((pow_max-pow_min)*y + pow_min, 1./(slope+1.))

total_mass = 0.
while total_mass < surface_density*(boxsize**2):
    radius = powerlaw(slope=-3, min_v=1, max_v=4)  # [m]
    mass = particle_density*4./3.*np.pi*(radius**3)
    x = np.random.uniform(low=-boxsize/2., high=boxsize/2.)
    sim.add(
        m=mass,
        r=radius,
        x=x,
        y=np.random.uniform(low=-boxsize/2., high=boxsize/2.),
        z=np.random.normal(),
        vx = 0.,
        vy = -3./2.*x*OMEGA,
        vz = 0.)
    total_mass += mass

import matplotlib.pyplot as plt
import matplotlib.patches as patches
def plotParticles(sim):
    fig = plt.figure(figsize=(8,8))
    ax = plt.subplot(111,aspect='equal')
    ax.set_ylabel("radial coordinate [m]")
    ax.set_xlabel("azimuthal coordinate [m]")
    ax.set_ylim(-boxsize/2.,boxsize/2.)
    ax.set_xlim(-boxsize/2.,boxsize/2.)

    for i, p in enumerate(sim.particles):
        circ = patches.Circle((p.y, p.x), p.r,
          facecolor='darkgray', edgecolor='black')
        ax.add_patch(circ)

plotParticles(sim)
sim.integrate(2.*np.pi/OMEGA)
plotParticles(sim)
plt.show()
```